

Using moisture conservation to evaluate oceanic surface freshwater fluxes in climate models

J. M. Rodríguez · T. C. Johns · R. B. Thorpe ·
A. Wiltshire

Received: 3 December 2009 / Accepted: 17 August 2010 / Published online: 10 September 2010
© Her Majesty the Queen in Right of Canada 2010

Abstract We apply a diagnostic based on moisture conservation in the atmosphere, integrated over planetary-scale ocean basins and drainage areas to evaluate freshwater fluxes over the ocean surface to three generations of the Hadley Centre climate model (HadCM3, HadGEM1 and HadGEM2-AO). The coherent inclusion of runoff by the diagnostic enables model surface freshwater fluxes to be compared directly with observational estimates of precipitation, evaporation and river discharge. We also introduce a normalised metric, based on model-observation RMS differences, to assess the representation of the fluxes by the model. This methodology could be a powerful tool for evaluating model performance during future model development and model intercomparison exercises. Using this diagnostic, and defining the drainage areas from the global river routing model TRIP, we obtain large-scale surface oceanic fluxes from ERA40 and NCAR-NCEP reanalysis data, which we compare with analogous budgets computed from a set of individual observational estimates of evaporation, precipitation and river discharge. The sum of errors in the Hadley Centre climate model in all ocean basins suggests a steady improvement over the three generations of the model. However, an analysis of sources and sinks of water vapour shows common errors in the models, like an excess of evaporation in the tropical-subtropical Atlantic, and a surplus of water vapour export from tropical-subtropical areas to the mid-latitude regions, making the oceanic surface fluxes too fresh at mid latitudes. Errors in

the models are consistent with an excessively strong hydrological cycle.

Keywords Large-scale ocean-atmosphere interactions · Global hydrological cycle · Climate model evaluation

1 Introduction

Knowledge of the hydrological cycle is essential for an understanding of the climate system of our planet. Water influences the climate through various processes in all components of the system and couplings between them (Chahine 1992; Oki 1999; Trenberth et al. 2007). In the atmosphere, water vapour absorbs both shortwave and longwave radiation. It also contributes to the heat budget in the form of transport of latent heat. The release of latent heat by condensation heats up the atmosphere and affects its general circulation.

On the other hand, the density structure of the ocean is strongly influenced by the salinity distribution, especially in cold regions. The transport of freshwater in the sea and the transport of water vapour in the atmosphere are coupled and constitute a significant feedback on climate. The oceanic thermohaline circulation (THC) is one of the major mechanisms in the climate system. Studies suggest that the strength of the overturning of this circulation may be related to density gradients in the Atlantic Ocean (Park 1999; Thorpe et al. 2001). Salinity distributions in the Atlantic Ocean are caused in part by the imbalance of evaporation, precipitation and river runoff and could be strongly affected by the transport of atmospheric freshwater.

Global warming is likely to intensify the global hydrological cycle and bring changes to the water vapour transport, changing the magnitude and spatial distribution

J. M. Rodríguez (✉) · T. C. Johns · R. B. Thorpe · A. Wiltshire
Hadley Centre for Climate Prediction and Research,
Met Office, FitzRoy Road,
Exeter EX1 3PB, UK
e-mail: jose.rodriguez@metoffice.gov.uk

of freshwater fluxes between atmosphere, land and sea-ice onto the ocean (Bosilovich et al. 2005; Held and Soden 2006). This, in turn, will modify the salinity distribution at the surface of the ocean and could potentially alter the ocean circulation through effects on its density. An appropriate representation of these fluxes by GCMs is essential to make confident projections of future characteristics of the THC, in particular its stability, under global warming conditions. It is therefore very important to investigate the skill of climate models to simulate large-scale water vapour transports and their mechanisms.

Any attempt to validate model simulations of large-scale aspects of the hydrological cycle is hindered by the lack of availability of relevant observations at those scales, in particular over the oceans. Furthermore, dissimilar climatologies of individual components of the hydrological cycle often have to be used in the assessment process. Certain combinations may exhibit considerable imbalances and large uncertainties. For instance, Edwards (2007) has evaluated the consistency with which the hydrological and energy cycles are represented by conventional climatologies. Using various combinations of observational estimates and reanalyses he has found that the imbalances in the hydrological cycle over the ocean represented by those estimates span a range of ± 0.45 mm/day in the mean, while rms errors lie between 0.87 and 1.74 mm/day.

Surface fluxes, in general, have to be estimated by indirect methods. One common approach is to apply the conservation equation of quantities like moisture, energy and momentum, and infer the fluxes as a residual, after computing the other variables in the budget equation (Trenberth 1997). Surface freshwater fluxes may be obtained this way from moisture balance in the atmosphere. The accuracy of the estimation of fluxes will depend critically on the quality of the atmospheric data. When considering fluxes at a global scale, a preferred option is to use global reanalyses.

In this paper we assess the simulations of large-scale atmospheric freshwater transports in three generations of the Hadley Centre climate model. We apply a diagnostic, derived from moisture conservation in the atmosphere, in combination with river basins defined in the global river channel network TRIP (Oki and Sud 1998), to evaluate the modelled surface freshwater fluxes over the ocean basins. We use data from ERA40 (Uppala et al. 2005) and NCAR-NCEP (Kalnay et al. 1996) to validate the models. The remainder of this paper is divided up into the following sections. In Sect. 2 we present a short review of water balance in the atmosphere and a derivation of the diagnostic. A metric to evaluate model performance against observations is introduced in this section. In Sect. 3 the models used are described. Results from models and reanalyses are presented in Sect. 4. We also compare in this section the surface fluxes obtained using our diagnostic and

reanalysis data with budgets derived from separate observational estimates of evaporation, precipitation and river runoff. Section 5 provides summary and conclusions.

2 Methodology

2.1 Water balance in the atmosphere

Water conservation in the climate system has been treated in various places, e.g., Peixoto and Oort (1992), Chen et al. (1994), Dodd and James (1996), Oki (1999). Our discussion in this section follows Chen et al. (1994). To a good approximation, water is conserved in the atmosphere, i.e., neglecting water loss through photo dissociation by solar radiation, and if fluxes at the surface are taken into account. This conservation is usually represented with an equation that involves vertically-integrated quantities:

$$\frac{\partial W_t}{\partial t} + \nabla_H \cdot \mathbf{Q}_t = E - P, \quad (1)$$

where W_t and \mathbf{Q}_t are respectively the total amount of water (vapour and condensed) and the total horizontal water flux in a unit area column:

$$W_t = W + W_c = \int_{z_0}^{\infty} \rho q dz + \int_{z_0}^{\infty} \rho q_c dz \quad (2)$$

$$\mathbf{Q}_t = \mathbf{Q} + \mathbf{Q}_c = \int_{z_0}^{\infty} \rho q \mathbf{v} dz + \int_{z_0}^{\infty} \rho q_c \mathbf{v} dz \quad (3)$$

ρq and ρq_c in the above expressions are respectively the mass of water vapour and condensed water (liquid and solid) per unit volume of the atmosphere. ∇_H is the horizontal divergence operator and E and P denote, respectively, evaporation and precipitation at the earth's surface.

The contribution from condensates to the water budget, although on occasions locally significant, is in general considerably smaller than that from water vapour on the global scale and can be neglected. Thus, water balance in the atmosphere can be approximated by conservation of water vapour:

$$\frac{\partial W}{\partial t} + \nabla_H \cdot \mathbf{Q} = E - P, \quad (4)$$

Excess of evaporation over precipitation is balanced by the local rate of change of water vapour storage and the loss through horizontal advection.

Further approximations can be made after time averaging the above equation. Changes in local precipitable water are very small on annual time scales compared to $E - P$ fluxes. After averaging the balance equation over periods of this length it simplifies to:

$$\nabla_H \cdot \bar{\mathbf{Q}} = \bar{E} - \bar{P}, \tag{5}$$

where the bars denote averaging in time. Water conservation in the above form has been used to estimate surface fluxes like evaporation and precipitation as residuals from atmospheric water vapour convergence.

2.2 Connection with the terrestrial and oceanic branches

Water balance at the land surface can be expressed as

$$\frac{\partial W_l}{\partial t} + \nabla_H \cdot \mathbf{F}_l = P - E, \tag{6}$$

where W_l represents the water storage and $\nabla_H \cdot \mathbf{F}_l$ is the horizontal water flux, including surface runoff and ground water movement. Generally, estimating the ground water movement is not easy. Its contribution in a large scale is presumed to be relatively small (Oki 1999).

Water conservation in the ocean is described by the equation

$$\frac{\partial W_o}{\partial t} + \nabla_H \cdot \mathbf{F}_o = P - E, \tag{7}$$

where W_o and $\nabla_H \cdot \mathbf{F}_o$ represent the freshwater storage and total horizontal freshwater flux, respectively. On land, changes in the water storage are generally small to be neglected in annual or longer averages. In the ocean, on the other hand, the freshwater storage may change at rates comparable with $P - E$ over long time scales (Pardaens et al. 2003). When time averaging is done over timescales on which that term can be neglected, the conservation equations for the land surface and oceanic branches have an analogous form to the atmospheric water conservation (5):

$$\nabla_H \cdot \bar{\mathbf{F}}_l = \bar{P} - \bar{E}, \tag{8}$$

$$\nabla_H \cdot \bar{\mathbf{F}}_o = \bar{P} - \bar{E}, \tag{9}$$

The term $\bar{E} - \bar{P}$ is common to all the balance equations above and connects the atmospheric, terrestrial and oceanic branches of the hydrological cycle.

To study regional budgets, it is convenient to integrate the conservation equations over the region of interest. We are interested in calculating the surface moisture fluxes that go into an ocean basin. The appropriate domain of integration in this case is the surface of the ocean basin and its adjacent land drainage area. We will denote them by A and C , respectively. Integrating Eq. (5) over A and (8) over C leads to:

$$\oint_{\partial A} \bar{\mathbf{Q}} \cdot \hat{\mathbf{n}} dr = \int_A (\bar{E} - \bar{P}) dA, \tag{10}$$

$$\oint_{\partial C} \bar{\mathbf{F}}_l \cdot \hat{\mathbf{n}} dr = \int_C (\bar{P} - \bar{E}) dA, \tag{11}$$

where $\hat{\mathbf{n}}$ is the outward unit vector normal to the domain boundary, and the left hand side of Eq. (11) is the net river discharge into the ocean basin, $\langle \bar{\mathbf{R}} \rangle_A$. Thus, the atmospheric and land freshwater fluxes going into an ocean basin can be obtained by computing the net water vapour flux across the boundary of the region defined by its surface and adjacent drainage area:

$$\begin{aligned} \oint_{\partial AUC} \bar{\mathbf{Q}} \cdot \hat{\mathbf{n}} dr &= \int_{AUC} (\bar{E} - \bar{P}) dA \\ &= \int_A (\bar{E} - \bar{P}) dA - \oint_{\partial C} \bar{\mathbf{F}}_l \cdot \hat{\mathbf{n}} dr \\ &\equiv \langle \bar{E} \rangle_A - \langle \bar{P} \rangle_A - \langle \bar{\mathbf{R}} \rangle_A \end{aligned} \tag{12}$$

Brackets indicate integration over the ocean surface A . An important element to consider when applying this method to calculate the surface fluxes is the definition of the drainage areas at planetary scales. Global river routing models may be used for this purpose. They are digital global river channel networks that calculate the discharge at each grid point. The river pathways are usually produced from digital elevation maps (DEMs) by a combination of automation and manual alteration.

To examine the global representation of water vapour fluxes by the climate models, we divided the globe into large-scale ocean basins and drainage areas, and compute the water vapour fluxes, $\int_l \mathbf{Q} \cdot \hat{\mathbf{n}} dr$, across every dividing segment between areas, as shown in Fig. 1. The drainage basins have been derived from the global river channel network defined in TRIP, the river routing model developed by Oki and Sud (1998). TRIP defines the actual river catchment areas in two of the models analysed, HadGEM1 and HadGEM2-AO. There is no unique way to construct the ocean drainage areas. There are locations on the land surface where the runoff does not go to the sea. The net water vapour flux across such regions is nil. Thus, we have the freedom to incorporate these inland-basin regions to any ocean drainage area without affecting the diagnosed freshwater flux into the corresponding ocean basin. Figure 1 shows the choices we have made. Quantities from the climate models and validating reanalyses have been interpolated to TRIP's $1^\circ \times 1^\circ$ grid. All calculations have been made in that grid. The vertically integrated moisture flux \mathbf{Q} is taken directly as a reanalysis product and as a diagnostic from GCMs. In the GCMs it has been calculated from values at model time-steps and then averaged to obtain the climatological values. In ERA40 the vertical integrals have been calculated from instantaneous model-level data at 6-hourly resolution and then averaged into monthly means. In NCEP/NCAR, monthly means of the integrand have been produced from instantaneous 6-hourly data before the vertical sum is performed. Fluxes estimated

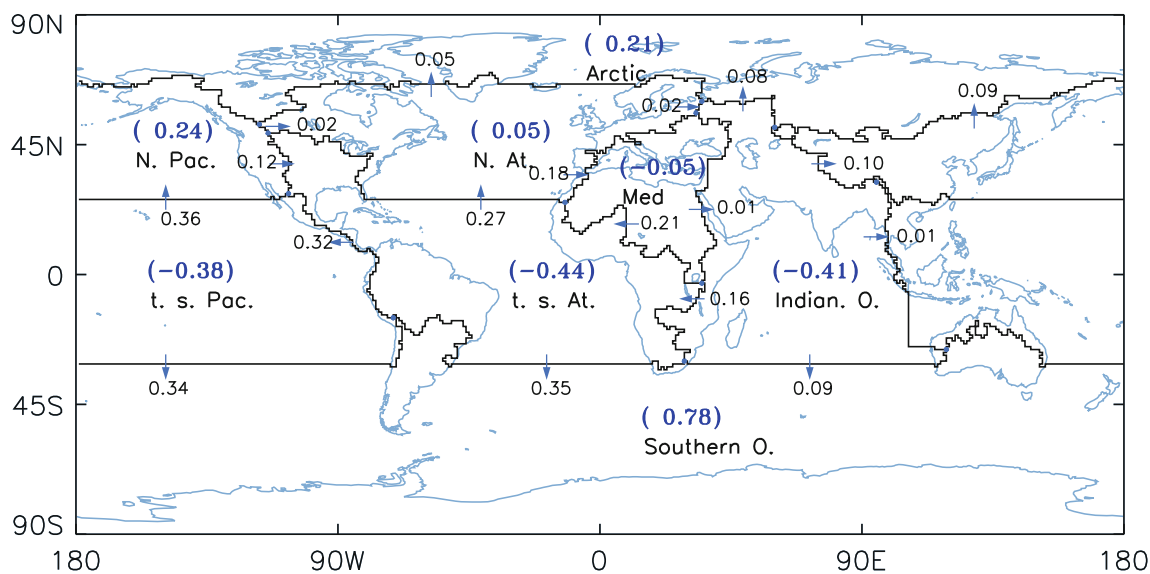


Fig. 1 Global distribution of water vapour fluxes (Sv). ERA 40 reanalysis. The flux shown next to an *arrow* has been integrated between the *blue dots* on a bounding segment. The sum of incoming

fluxes across the boundary of each defined region is shown in *blue*. In a climatological state they are equal to $P - E + R$ on the corresponding ocean basin

with the diagnostic presented here are *implied fluxes*. That is, they represent what is required to balance the surface exchange of water. GCMs and observations, on the other hand, may suffer from imbalances and biases, introducing errors in the estimations. In the case of the reanalyses, the sampling used to calculate the means and the data assimilation process, where the model atmosphere is adjusted to fit observations, produce data that is not necessarily in balance.

2.3 A metric to evaluate GCMs

In this study we use a metric to evaluate the model surface freshwater fluxes against reanalysis data and to quantify improvements in the representation of these fluxes over the different configurations of the model.

For each large-scale ocean basin we estimate the model and observation surface fluxes. We denote them by f_M and f_O respectively. We define E_M as the temporal RMS difference in surface fluxes between model and observational estimates:

$$E_M = \left[\frac{1}{N} \sum_{i=1}^N (f_M - f_O)_i^2 \right]^{\frac{1}{2}} \quad (13)$$

The results are normalised by a similar RMS difference from a reference model and we define a metric

$$S_M = \frac{E_M}{E_R} \quad (14)$$

If $0 < S_M < 1$, the model we are evaluating performs better than the reference model against the selected observations.

If $S_M \approx 1$, the model performs similarly to the reference model, and if $S_M \gg 1$, the model performance is poorer than the reference model. The observational uncertainty can also be partly taken into account by using a second set of observations and calculating the RMS difference between observational fluxes:

$$U = \left[\frac{1}{N} \sum_{i=1}^N (f_{O_1} - f_{O_2})_i^2 \right]^{\frac{1}{2}} \quad (15)$$

The uncertainty estimate is also normalised by the reference model:

$$S_U = \frac{U}{E_R} \quad (16)$$

If $S_M < S_U$, the model performance is within the observational uncertainty. In this study we use ERA40 and NCAR-NCEP as the first and second sets of observational estimates. Series of 21 annual means have been used to calculate the RMS differences. The reanalysis data used corresponds to the 1979–2000 period.

3 Model descriptions

The models used in this study are the Hadley Centre climate models HadCM3, HadGEM1 and HadGEM2-AO, run with fixed 1860 forcings of greenhouse gases, ozone, sulphur and other aerosol emissions. Control runs of this type are used in the climate model community to study climate processes, for model evaluation and in detection and attribution analysis. Differences in water vapour transport

from these pre-industrial runs and twentieth-century simulations are small relative to observational uncertainties, making valid comparisons between these models and present-day observations possible.

3.1 HadCM3

HadCM3 is the Hadley Centre global coupled climate model. The atmosphere component has a resolution of 3.75° longitude by 2.5° latitude with 19 vertical levels. The ocean component has a resolution of $1.25^\circ \times 1.25^\circ$ longitude by latitude with 20 vertical levels, and it is based on the Bryan-Cox model (Bryan 1969; Cox 1984). HadCM3 has a sea ice component with thermodynamics based on the zero-layer model of Semtner (1976) and includes simple parameterizations of ice drift and leads. A detailed description of the different components of HadCM3 and their physical schemes can be found in Gordon et al. (2000) and Pope et al. (2000).

3.2 HadGEM1

HadGEM1 is the Hadley Centre Global Environmental Model version 1 (Johns et al. 2006). The model has a non hydrostatic atmospheric dynamical core that uses a semi-implicit, semi-Lagrangian time integration scheme. The standard atmospheric component uses a horizontal resolution of $1.25^\circ \times 1.875^\circ$ longitude by latitude, with 38 layers in the vertical extending to 39 km in height. A river routing model, TRIP (Oki and Sud 1998), has been introduced, which includes river transport dynamics, determined by fluxes of surface and subsurface runoff. For a detailed description of the atmospheric component of the model and its performance see Martin et al. (2006) and Ringer et al. (2006).

The oceanic component of HadGEM1 has a variable horizontal resolution: a fixed zonal resolution of 1° and meridional resolution of 1° between the poles and 30° latitude from which it increases smoothly to $\frac{1}{3}^\circ$ at the Equator. The model has 40 levels in the vertical, spaced irregularly with a thickness of 10 m near the surface. The evolution of sea ice thickness is determined by thermodynamic growth/melt, advection and redistribution by ridging. HadGEM1 uses the Los Alamos National Laboratory sea ice (CICE) model ice ridging scheme (Hunke and Lipscomb 2004).

3.3 HadGEM2-AO

HadGEM2-AO (Collins et al. 2008) uses the same dynamical core as HadGEM1 and is run at the same horizontal and vertical resolutions in both the atmosphere and ocean. The main changes in the model are associated with

physical processes. In the atmosphere, an adaptive detrainment parameterization in the convection scheme has been implemented, which has improved the simulation of tropical convection. The treatment of excess water from super-saturated soil surfaces has been changed, a background climatology of biogenic aerosols has been included, and improvements in the representation of the lifetime of convective clouds have been implemented, all of which have led to reductions in a land surface warm bias over northern continents. In the ocean, the background ocean diffusivity profile in the thermocline has been changed, which has substantially reduced an SST bias in the tropics.

4 Results

4.1 Results from ERA40 and NCAR-NCEP

In this subsection we show the use of the diagnostic described in Sect. 2 to estimate the freshwater fluxes from the atmosphere and land surface over large-scale ocean basins. We first apply the diagnostic to ERA40 and NCAR-NCEP data and then compare the surface fluxes obtained this way with various combinations of independent observational estimates of evaporation, precipitation and river discharge.

Figures 1 and 2 show the global distribution of water vapour fluxes diagnosed from ERA40 and NCAR-NCEP data, respectively. The main features of these transports are shared by both climatologies. To a large extent the flow of water vapour portrays the general circulation in the lower troposphere: easterlies in the tropical belt, westerlies in mid-latitudes and the meridional flux is predominantly poleward throughout the year. In particular, in the tropical-subtropical Atlantic region freshwater is imported across Africa and exported to the Pacific across Central America. Westerly flow brings input of vapour to the North Atlantic basin across the American boundary, and freshwater is lost across the African and European continents.

In a climatological state the sum of water vapour fluxes across the boundaries of each region defined in Figs. 1 and 2 is equivalent to the surface freshwater fluxes on the corresponding ocean basin. These fluxes have been summarised in Table 1, where a series of 21 consecutive years have been used to produce mean values and standard deviations. There's a good amount of overlap between the estimates in both climatologies for most of the ocean basins. The exceptions are the Arctic region, where NCAR-NCEP data show a larger excess in precipitation than ERA40 data, and the North Pacific basin, where the forcings are fresher in ERA40 than in NCAR-NCEP.

In order to validate these estimates, we have compared them against combinations of individual P , E and R

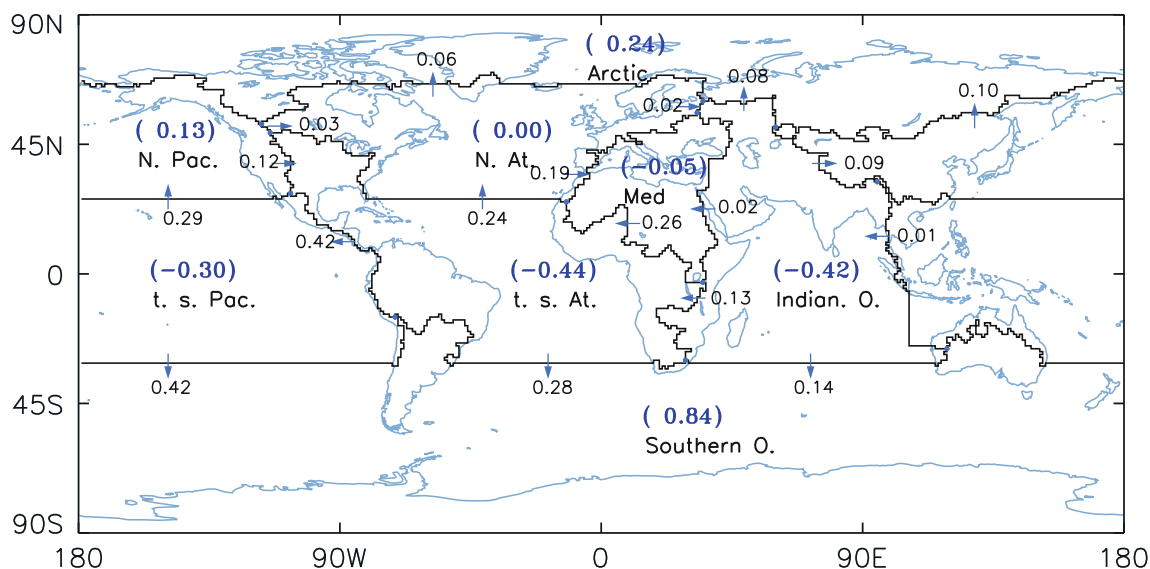


Fig. 2 Same as in Fig. 1. NCAR-NCEP reanalysis

Table 1 Diagnosed surface freshwater fluxes, $P - E + R$ from ERA40 and NCAR-NCEP reanalyses (Sv)

Ocean basin	ERA40	NCAR-NCEP
Arctic	0.21 ± 0.01	0.24 ± 0.01
North Atlantic	0.05 ± 0.03	0.00 ± 0.03
Trop./Subtrop. Atlantic	-0.44 ± 0.08	-0.44 ± 0.05
Mediterranean Sea	-0.05 ± 0.03	-0.05 ± 0.01
North Pacific	0.24 ± 0.03	0.13 ± 0.03
Trop./Subtrop. Pacific	-0.38 ± 0.08	-0.30 ± 0.08
Indian Ocean	-0.41 ± 0.06	-0.42 ± 0.04
Southern Ocean	0.78 ± 0.04	0.84 ± 0.05

The table shows 1979–2000 averages and $2\text{-}\sigma$ uncertainties

estimates. We will briefly describe the climatologies employed for such a comparison. A detailed analysis of biases and errors in latent heat and precipitation observations can be found in Edwards (2007).

For evaporation, data from latent heat climatologies NOC1.1a (Grist and Josey 2003), GSSTF2.0 (Chou et al. 2003, 2004) and da Silva (da Silva et al. 1994) were used and converted using a constant coefficient. NOC1.1a is based on observations taken from ships. It is derived from NOC1.1 climatology (Josey et al. 1999) by applying constraints derived from estimates of oceanic heat transport. GSSTF2.0 is a satellite-based climatology, with data obtained from the Special Sensor Microwave Imager (SSM/I). It uses bulk flux formulae to obtain surface fluxes. The da Silva climatology is derived from surface marine data. The climatological fields are produced using data from COADS.

For precipitation we have used CMAP (Xie and Arkin 1997) and GPCP2 (Adler et al. 2003). Both climatologies are derived by combining data from rain gauges and

satellites. The main differences between them are found over the oceans (Edwards 2007).

The climatologies used to estimate the river discharges are GRDC (Global Runoff Data Centre 2009), Baumgartner and Reichel (1975) and Dai and Trenberth (2002). The runoff into the ocean is derived from discharge stations and estimations of runoff on areas not captured by the stations.

Figure 3 shows the surface fluxes, $P - E + R$, for combinations of the different climatologies. The choices of river discharges are indicated by the symbols. The choices of evaporation, by the symbol colors, and the choices of precipitation, by the sizes of symbols. For comparison, we include the values of budgets obtained with our conservative diagnostic using reanalysis data.

The first thing to notice is the large spread in the values of surface fluxes from the hybrid climatologies. In general, the main differences in the freshwater budgets are given by differences in evaporation and precipitation data. By comparison, the spread of the surface fluxes obtained with our diagnostic is much smaller. Their values comfortably fall within the inter-climatology spread. There are large imbalances of freshwater when combinations of disparate climatologies are used. This is represented in the figure by non vanishing values in the global budget. Those imbalances vary from -1.8 Sv to 1.0 Sv. The figure shows that the data split into two cases of imbalance. Combinations using da Silva climatology for evaporation, (black symbols in Fig. 3), have a positive (precipitative) imbalance, the rest a negative (evaporative) imbalance. The global budget estimated with our diagnostic, on the other hand, is zero by construction.

Edwards has found that combinations of climatologies show the largest inconsistencies in the tropical regions

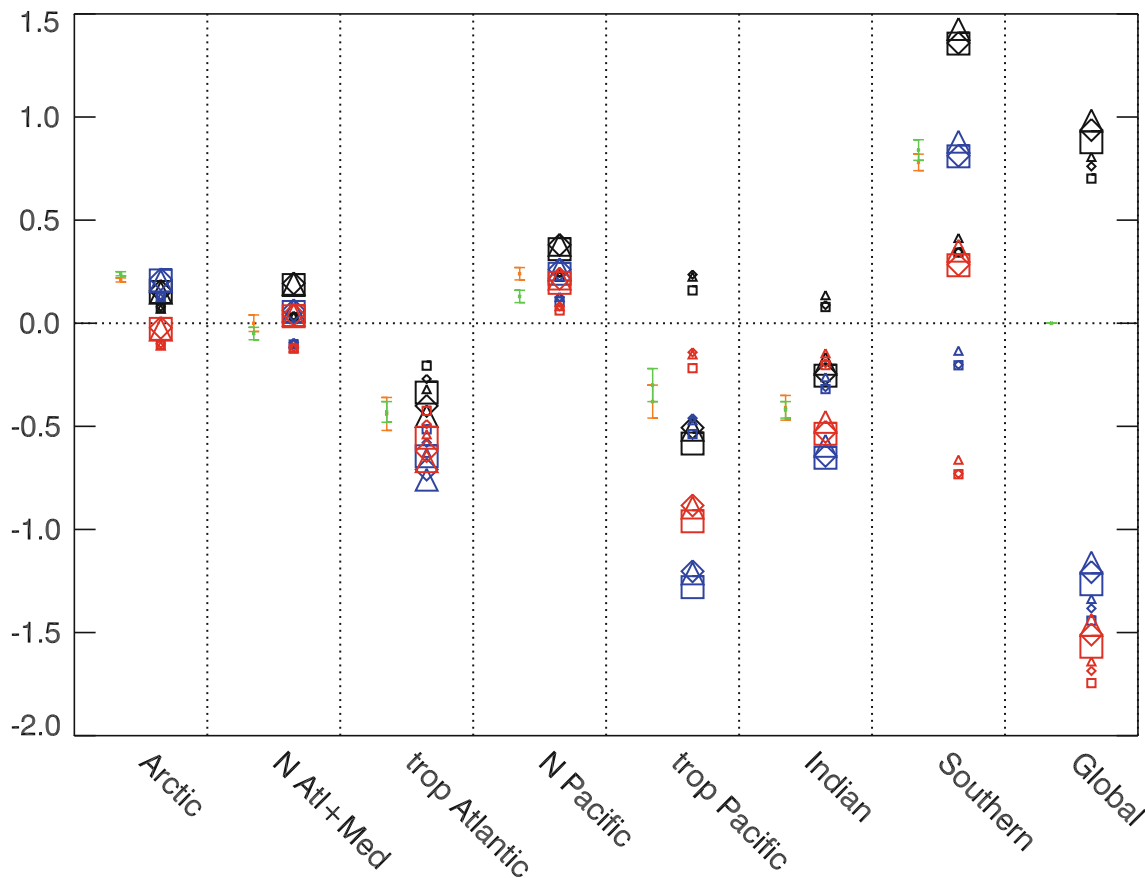


Fig. 3 Oceanic surface freshwater fluxes, $P - E + R$, (Sv). Symbols denote river discharge climatologies. Diamonds GRDC, squares Dai-Trenberth, triangles Baumgartner-Reichel. Sizes of symbols denote precipitation climatologies. Small CMAP, large GPCP2. Color of

symbols denote evaporation climatologies. Black da Silva, red GSSTF2, blue NOC1.1a. For comparison, 1979–2000 averages and $2\text{-}\sigma$ uncertainties of estimates from reanalysis data are included. Orange ERA40, green: NCAR-NCEP

(Edwards 2007). This is also manifested in the surface fluxes over the oceans that we are analyzing here. In the evaporative regions of the Indian Ocean and tropical-subtropical Pacific the da Silva and CMAP combination, (small, black symbols in Fig. 3), gives estimates with an excess of precipitation. This is most likely the effect of the lower values of evaporation that the da Silva climatology shows in the tropical belt. Budgets in the tropical-subtropical Atlantic, on the other hand, show an excess of evaporation for all combinations.

At midlatitudes the spread of estimates using our diagnostic is more comparable with the narrower spread of values from observational estimates. This agrees with Edwards findings of better consistency in recent climatologies at midlatitudes.

There is a very large uncertainty in the hybrid budgets at the Southern Ocean. Combinations using CMAP for precipitation, and NOC1.1a and GSSTF2.0 for evaporation, (small, blue and red symbols in Fig. 3), give an excess of evaporation over precipitation. This is likely due to CMAP’s underestimation of precipitation in this region

(Edwards 2007). In the Arctic, climatological combinations with GSSTF2.0 (red symbols), give excess of evaporation over precipitation. The other combinations produce excess of precipitation over evaporation. Estimations using evaporation from NOC1.1a have the handicap that the evaporation climatology has missing data in most of this region.

4.2 Results from GCMs

Twenty-one-year means of water vapour fluxes over the large-scale regions are shown in Figs. 4, 5 and 6. Their corresponding oceanic surface water fluxes are summarised in Table 2.

The main patterns of the water vapour transports in the GCMs are analogous to the ERA40 and NCAR-NCEP transports, reflecting the general circulation in the lower troposphere. Compared to the reanalyses, the models show an excess of evaporation in the tropical-subtropical Atlantic. This is manifested mainly as a lack of water vapour imported across the African boundary. HadCM3 model, which has a significant evaporative bias in this

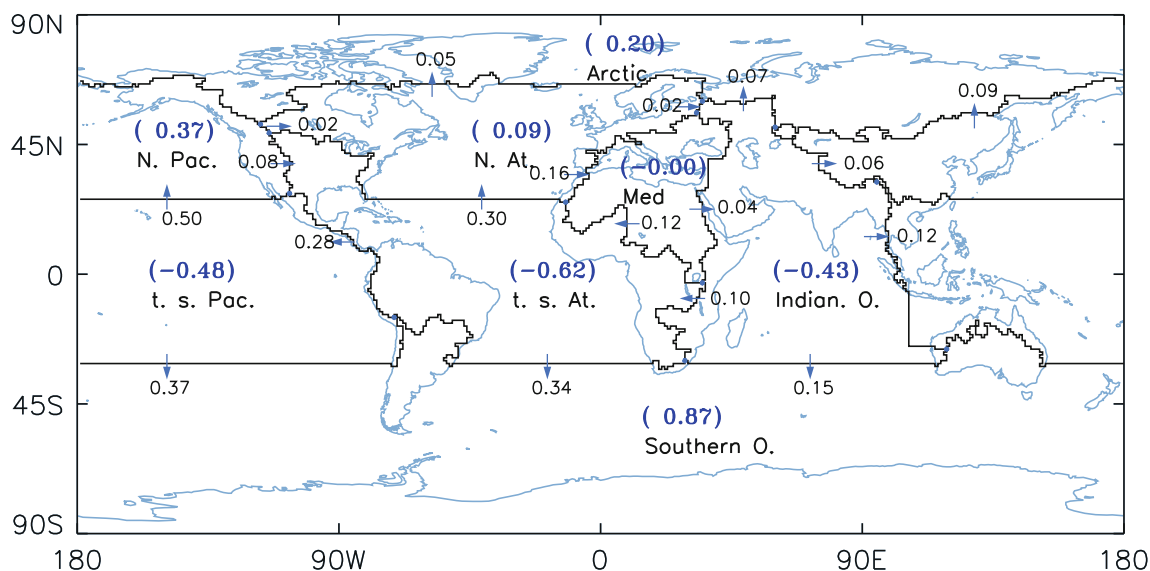


Fig. 4 Transport of water vapour into ocean basins(Sv). HadGEM2-AO

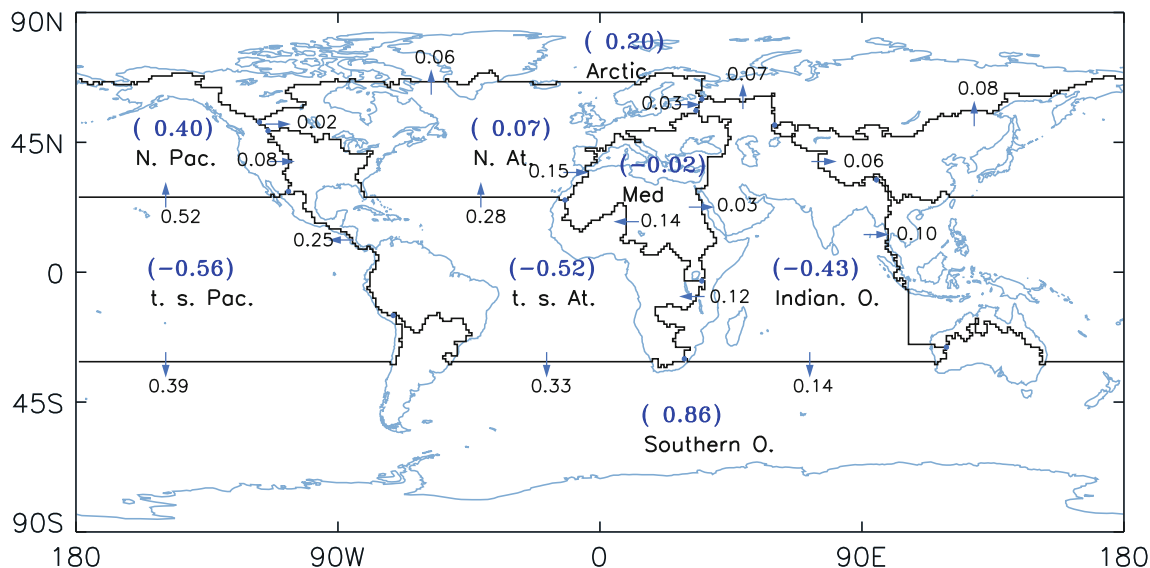


Fig. 5 Transport of water vapour into ocean basins(Sv). HadGEM1

region (Pardaens et al. 2003), also shows a large export to the Pacific Ocean. Models have difficulties in representing the surface fluxes over the tropical-subtropical Pacific. HadCM3 displays a fresh bias in this area, whereas HadGEM1 and HadGEM2-AO an evaporative error. The freshwater budget in this region in all three models suffers from too much import of water vapour across the Indonesia boundary and an excessive export of water vapour to the mid-latitude regions. This surplus of water vapour from the tropical-subtropical regions makes, in turn, the surface fluxes over the oceans too fresh at mid latitudes and, in the case of HadGEM1 and HadGEM2-AO, also produces a fresh bias over the Southern Ocean.

For most of this paper we use expression (12) to calculate the oceanic water fluxes in terms of water vapour transport, and neglect the contribution from changes in water storage. This can be justified when using annual means or longer time averages, since those terms are small compared to the rest in the conservation equation. However, at shorter time scales, changes in water storage may be of the same order or larger. This is shown in Table 3, where climatological values of area-integrated estimates of changes in precipitable water and land storage are displayed for the various regions defined above. The observational estimates have been obtained as follows. Changes in precipitable water have been computed from ERA40

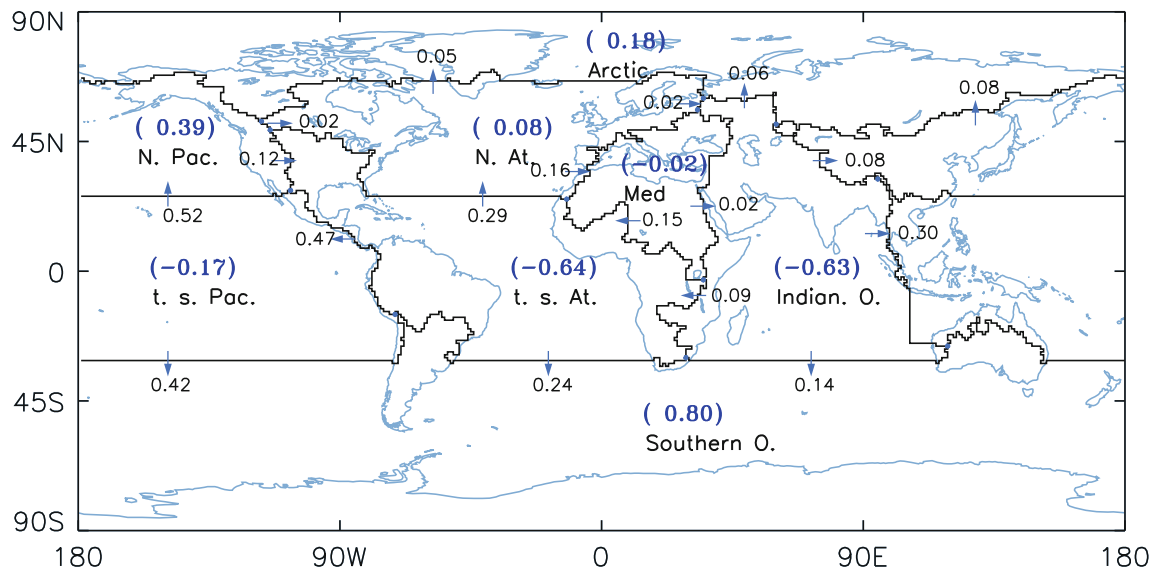


Fig. 6 Transport of water vapour into ocean basins (Sv). HadCM3

Table 2 Oceanic surface freshwater fluxes, $P - E + R$ from the GCMS (Sv)

Ocean basin	HadGEM2-AO	HadGEM1	HadCM3
Arctic	0.20 ± 0.01	0.20 ± 0.01	0.18 ± 0.01
North Atlantic	0.09 ± 0.02	0.07 ± 0.02	0.08 ± 0.02
Trop./Subtrop. Atlantic	-0.62 ± 0.04	-0.52 ± 0.04	-0.64 ± 0.07
Mediterranean Sea	0.00 ± 0.01	-0.02 ± 0.01	-0.02 ± 0.01
North Pacific	0.37 ± 0.02	0.40 ± 0.02	0.39 ± 0.03
Trop./Subtrop. Pacific	-0.48 ± 0.06	-0.56 ± 0.07	-0.17 ± 0.08
Indian Ocean	-0.43 ± 0.05	-0.43 ± 0.07	-0.63 ± 0.07
Southern Ocean	0.87 ± 0.02	0.86 ± 0.02	0.80 ± 0.02

The table shows climatological values and 2-σ uncertainties

Table 3 Maximum values of area-integrated monthly changes in precipitable water and land storage, (Sv)

Ocean basin	$\langle \frac{\partial W}{\partial t} \rangle$	$\langle \frac{\partial W_L}{\partial t} \rangle$
Arctic	0.06 (May)	-0.24 (Aug)
North Atlantic	0.06 (May)	-0.18 (Jul)
Trop./Subtrop. Atlantic	0.04 (Feb)	0.31 (Jan)
Mediterranean Sea	-0.04 (Oct)	-0.06 (Jun)
North Pacific	0.11 (May)	-0.07 (Jul)
Trop./Subtrop. Pacific	-0.04 (May)	-0.03 (Nov)
Indian Ocean	-0.04 (Aug)	-0.09 (Oct)
Southern Ocean	0.10 (Nov)	0.04 (Feb)

The months at which the values occur are shown in parentheses. We use the same nomenclature as in Sect. 2. Brackets indicate area integration

data. Changes in land water storage, on the other hand, consist of three components, changes in soil moisture, changes in the river channel storage and changes in snow cover. We have calculated the soil moisture budgets with data from CLM and Mosaic land surface models forced with observations (Mitchell et al. 2004). To obtain estimates of the change in river storage, the river routing model TRIP was forced with Fekete runoff climatology (Fekete et al. 2002). Change in snowcover was estimated using ERA40 snow depth with an assumed fixed snow density of 250 kg/m². The uncertainties in the observed components of land water storage are relatively large, partly due to the lack of direct observations and the reliance on reanalysis and model/data hybrid products.

The tendency terms show an annual cycle that, when averaged, has values of the order of 0.001 Sv or smaller. Changes in land storage are in general larger than changes

in precipitable water. Two of the considered regions show a pronounced annual cycle in their land storage budgets. The Arctic region, with its considerable amount of snow melting, and the tropical-subtropical Atlantic region, where the annual cycle reflects the motion of large water masses from the main rivers included in the region.

Figure 7 shows the annual cycle of the oceanic surface freshwater budgets from HadGEM2-AO, HadCM3 and the observational estimates. In most of the defined regions, the annual cycle is well represented by the GCMs (the curves from models and observational estimates have similar shapes), although GCM cycles show positive and negative biases. An exception is tropical-subtropical Pacific region. In the Arctic and North Atlantic regions, the main contribution to the annual cycle comes from the change in land water storage. In the Arctic, this cycle is better represented in HadGEM2-AO than in HadCM3. The large evaporative

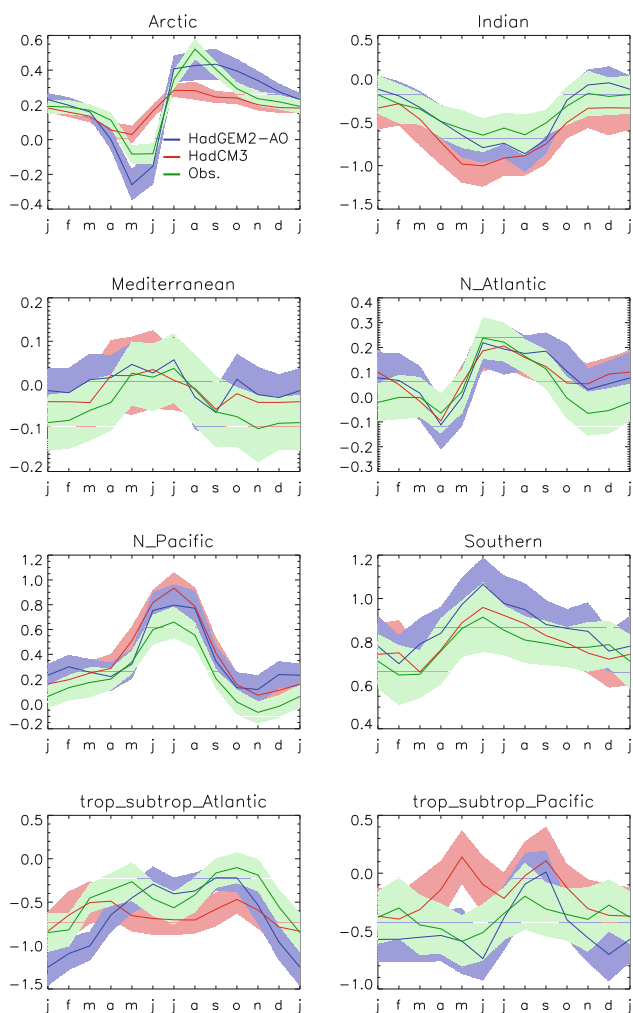


Fig. 7 Oceanic surface freshwater budgets, (Sv). Annual cycle. Blue HadGEM2-AO. Red HadCM3. Green Observational estimates. Shades indicate 2- σ uncertainty

bias shown by HadCM3 in the tropical-subtropical Atlantic is particularly noticeable during the April to October months. This bias has been reduced in HadGEM2-AO. For most of the defined regions, the annual cycle is better represented in HadGEM2-AO than in HadCM3, except in the Southern Ocean where the model has a positive bias all year round.

In order to quantify the errors in the oceanic surface freshwater budgets and to compare objectively the performance of the different GCMs, we have used the metric described in Sect. 2. Results are shown in Fig. 8, where S_M and S_U values on each large-scale ocean basin are displayed. There are large observational uncertainties relative to the reference model values, especially in the Arctic, North Atlantic and Southern Ocean. The model budgets are within the range of observational estimates only in the Arctic and North Atlantic regions. HadGEM2-AO scores better than HadGEM1 and HadCM3 in the majority of the

defined regions, with the exceptions of the Southern Ocean, North Atlantic and the tropical-subtropical Atlantic. In the last region, a compensation error in precipitation puts HadGEM1's fluxes closer to observational uncertainty. A substantial improvement in the freshwater budget over the Indian Ocean can be noticed in HadGEM1 and HadGEM2-AO, compared to HadCM3 values. A metric value for the sum of RMS differences in all regions has been included in this plot (denoted as Total in Fig. 8). It suggests steady improvement in the representation of the freshwater surface fluxes along the three generations of the model.

Metrics are useful to assess different aspects of a GCM, since they provide quantitative information of model performance and reduce subjectivity in the evaluation. However, they are less informative to shed light on the causes of errors. To complete the assessment of the model representation of water vapour transports we will present in the following subsections two aspects of their global hydrological cycle, the sources and sinks of water vapour and the strength of the hydrological cycle.

4.3 Water vapour divergence

The divergence field of the water vapour transport links sources and sinks of water vapour to evaporation and precipitation budgets (see, for example, Eq. (5) from Sect. 2). Divergent regions on the globe correspond to places where evaporation is greater than precipitation, whereas water vapour convergence is found in locations where precipitation exceeds evaporation. Figure 9a illustrates global water

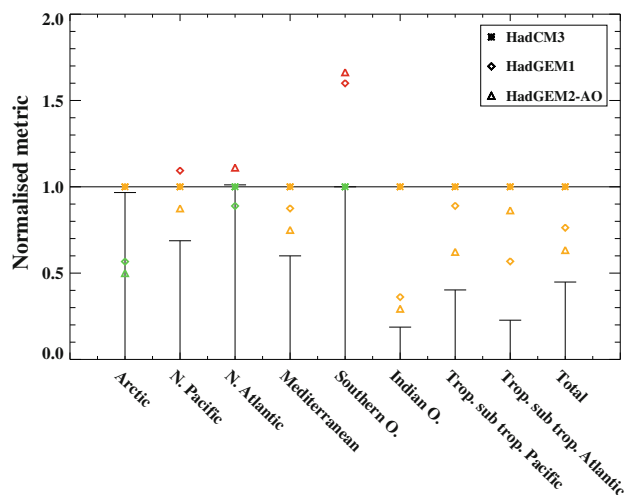


Fig. 8 Normalised metric to assess models. Observational uncertainties are indicated by error bars. The green color indicates that the model surface flux value is within observation uncertainty. Amber color indicates that the flux estimate is outside observation uncertainty, but closer to observations than the reference model. Red indicates that the flux is outside observation uncertainty and worse than the reference model. HadCM3 has been used as reference model

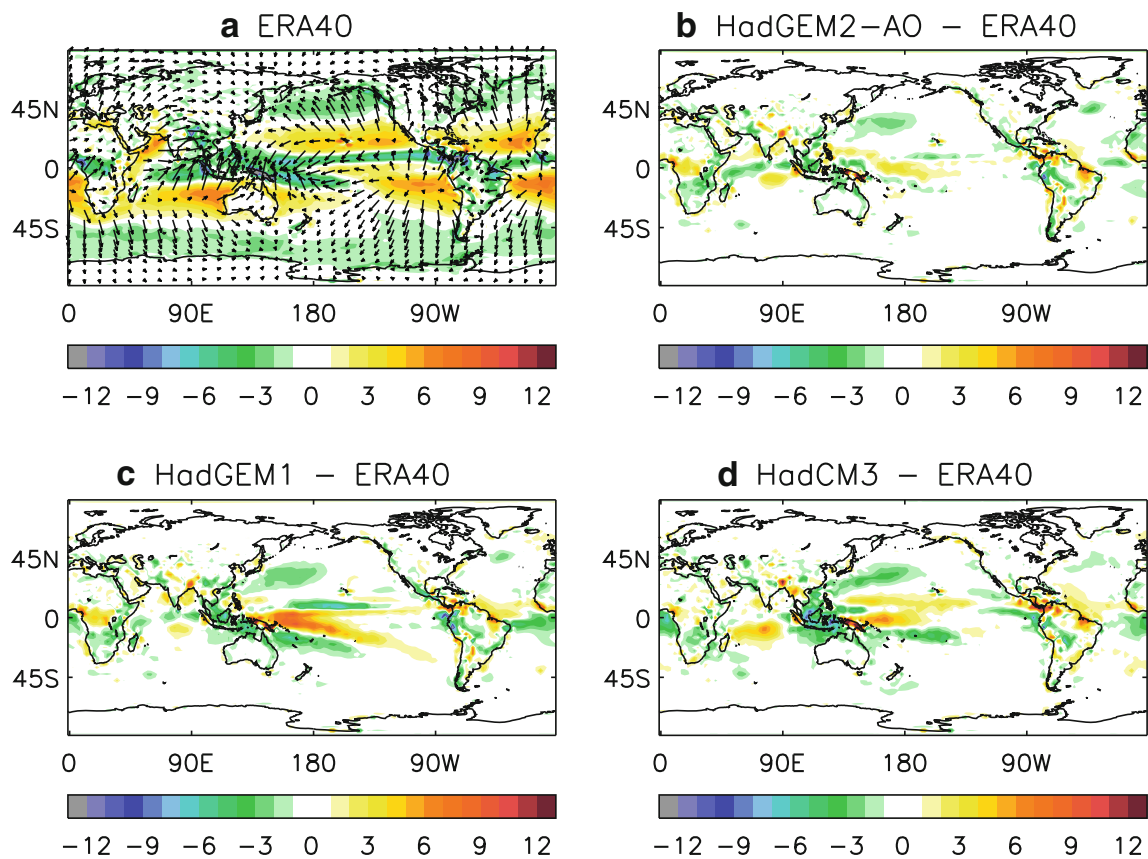


Fig. 9 a Sources and sinks of water vapour in ERA40. 1979–2000 average water vapour divergence (10^{-5} Kg/m²s) superimposed to the divergent component of the water vapour flux vector. b HadGEM2-AO $\bar{E} - \bar{P}$ error from ERA40, computed from their difference of water

vapour flux divergence (10^{-5} Kg/m²s). c HadGEM1 $\bar{E} - \bar{P}$ error. d HadCM3 $\bar{E} - \bar{P}$ error

vapour sources and sinks from ERA40 data. A climatological mean of water vapour divergence is superimposed to the divergent component of the water vapour flux vector. Sources are represented by yellow and orange shadings, whereas sinks, by green shadings. Water vapour source regions are situated in the Pacific and Atlantic subtropics as well as in the Indian Ocean region west of Australia and the centre of divergence west of India that supplies part of the moisture for the Indian monsoon. Sinks are located in the equatorial convective zones and mid to high latitudes, and are associated with the ITCZ and storm tracks respectively. Over land, the belts of convergence are placed on the drainage basins of the large river systems.

Figures 9b–d show the model $E - P$ errors from ERA40, obtained from their differences in the water vapour divergence. Green shading indicates a negative error, whereas yellow and orange shading show positive errors. All three generations of the coupled model show a large negative $E - P$ bias over the Maritime Continent, that is associated with a warm SST error in the region and a cold equatorial Pacific (Martin et al. 2006; Pardaens

et al. 2003). This is particularly exacerbated in HadGEM1 (see Fig. 9c). In this model the equatorial cooling is considerably larger than in the other model configurations. HadGEM1 is in a regime with excessive convection occurring over Indonesia and a stronger Walker circulation. The convection in that region is promoted by local warmer SSTs and by inhibiting convection in the equatorial Pacific, where the cold SST anomalies take place. The cold anomalies, on the other hand, are to a large extent originated by excessive easterly wind stress on the lower branch of the stronger Walker circulation (Martin et al. 2006). Those biases have diminished significantly in HadGEM2-AO, as shown in Fig. 9b. The adaptive detrainment parameterization included in the convective scheme of this configuration has improved the simulations of tropical convection and wind stress over the tropical Pacific. Changes in the background ocean diffusivity profile in the thermocline have substantially reduced the SST bias in the tropics.

Comparisons with individual climatologies of E and P show that the model errors in the tropical-subtropical

Atlantic region are characterized by an excess of evaporation in the equatorial and northern subtropic regions, an excess of precipitation over the equatorial Atlantic, and a lack of evaporation in the southern subtropic. Integrated over the area used to calculate the metric results presented in the last subsection, they manifest themselves as a positive $E - P$ bias. This bias is more prominent in HadCM3 and has been substantially reduced in HadGEM1 and HadGEM2-AO. Although the integrated $E - P$ budget over the area is closer to reanalysis values in HadGEM1, this is in part due to the excess of precipitation over the equatorial Atlantic. The spatial patterns of evaporation and precipitation on this area are better represented in HadGEM2-AO.

Over land the three model configurations show a lack of precipitation in the Amazon river basin, and a precipitation deficit in the equatorial African area is also displayed by the HadGEM models.

For all models, precipitation tends to be overestimated at mid to high latitudes. HadGEM2-AO, worsens the precipitative bias in the North Atlantic basin. Errors of this type lead to excessive freshwater forcing the surface waters of the ocean in these regions.

4.4 Precipitable water and strength of the hydrological cycle

The above errors in the surface freshwater fluxes are consistent with an excessively active water cycle modelled by the GCMs. As a measure of the strength of the hydrological cycle, we estimate the global residence time of water in the atmosphere by computing the rate at which water leaves the atmospheric storage (Bosilovich et al. 2005): $\tau = \frac{\langle W \rangle}{\langle P \rangle}$, where τ , $\langle W \rangle$ and $\langle P \rangle$ are respectively the residence time, the total amount of water vapour (global precipitable water) and the global precipitation. A comparison of model precipitable water and NVAP climatology (Randel et al. 1996) is shown in Fig. 10. In general the model represents well the main spatial patterns of the field: a continuous decrease from a maximum value in the equatorial regions to the North and South poles, with departures from zonal symmetry associated with topography, and small values of precipitable water in terrestrial zones of strong subsidence. However, the difference fields on Fig. 10b–d show a considerable deficit of model precipitable water in the tropics. The deficit in the tropical

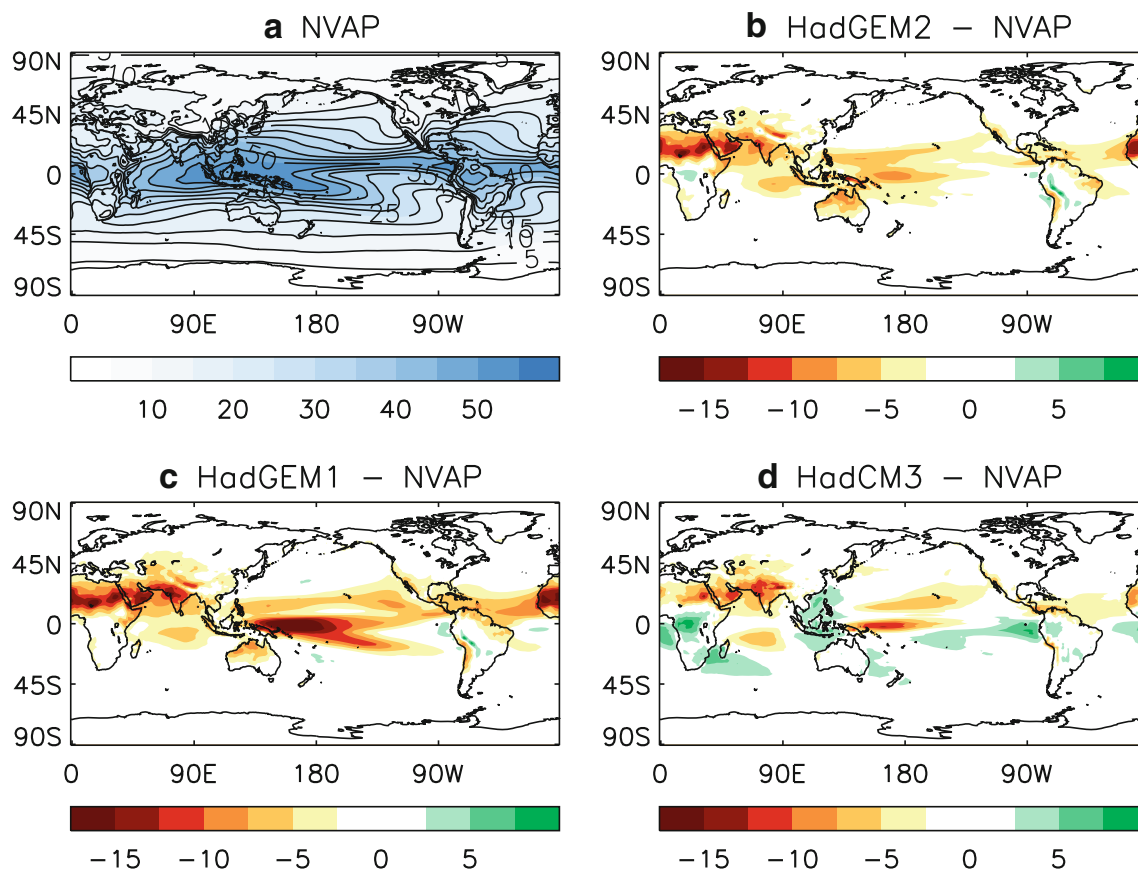


Fig. 10 a 1988–1998 NVAP precipitable water. b HadGEM2-AO minus NVAP precipitable water. c HadGEM1 minus NVAP precipitable water. d HadCM3 minus NVAP precipitable water. Values are expressed in mm

Table 4 Global values of precipitable water (10^{16} Kg), precipitation (10^{15} Kg/day) and water-vapour residence time (day)

	P. water	Precip.	Residence time
Climatology	1.25	1.33	9.39
HadGEM2-AO	1.14	1.57	7.27
HadGEM1	1.12	1.57	7.13
HadCM3	1.22	1.48	8.24
HadGEM2-A	1.19	1.56	7.65
HadGAM1	1.23	1.59	7.74
HadAM3	1.24	1.50	8.27

NVAP and GPCP2 have been used to estimate the climatology values of precipitable water and precipitation, respectively

Pacific is mainly caused by the cold bias in the region mentioned in the previous subsection. When the models are run in the atmosphere-only mode with prescribed SSTs, the moist deficit in the tropical Pacific is no longer present. Table 4 shows global values of precipitable water, precipitation and residence times for models and climatologies. The models show a deficit in the total amount of water vapour and a more intense global precipitation, compared to climatologies, leading to a shorter water vapour residence time. Water vapour recycles between 12 and 24% faster in the different configurations of the model. The atmospheric-only versions (HadGEM2-A, HadGAM1 and HadAM3) show global precipitable water close to the climatology value, but keep the same precipitation error as their coupled counterparts. In sum, the shorter global water vapour residence time that characterises the more active hydrological cycle modelled by the GCMs is mainly caused by a deficit in water vapour content over the tropical oceans and an enhanced global precipitation rate.

5 Summary and conclusions

We have analysed large-scale water vapour transports in three versions of the Hadley Centre global climate model. A diagnostic based on moisture conservation in the atmosphere has been used to derive surface freshwater budgets over ocean basins, employing integrated water vapour fluxes. This provides an effective tool to investigate model errors and biases.

Using the diagnostic we have estimated the oceanic surface freshwater budgets from ERA40 and NCAR-NCEP data. When compared, both reanalyses share the main features of water vapour transport and show a good amount of overlap in their values of surface freshwater fluxes for most of the ocean basins. The oceanic surface fluxes are also compatible with analogous budgets calculated from a set of various combinations of evaporation, precipitation and river discharge observational estimates. This is in part

due to the large uncertainty in the budgets obtained from the hybrid observations, which also show large global imbalances.

A metric has been introduced to evaluate the representation of the oceanic surface freshwater fluxes in the climate models. There are large observational uncertainties relative to reference model values. In general, HadGEM2-AO scores better than HadGEM1 and HadCM3. A noticeable exception is given over the Southern Ocean, where excessive import of water vapour from the Indo-Pacific region in HadGEM2-AO makes the atmospheric flux too fresh in this region.

An analysis of sources and sinks of water vapour reveals an excess of evaporation in the tropical-subtropical Atlantic shared by the three models. This is particularly large in HadCM3 and has been substantially reduced in HadGEM1 and HadGEM2-AO. The models also have difficulties in representing faithfully the seasonal cycle of surface fluxes over the tropical-subtropical Pacific. Another common error is a surplus of water vapour from the tropical-subtropical regions going into the mid-latitude regions. This makes the surface fluxes over the oceans too fresh at mid-latitudes.

The above errors are consistent with an excessively strong hydrological cycle. Water vapour recycles between 12% and 24% faster in the climate models, compared to estimates from observations. The shorter water vapour residence times in the GCMs are the effect of a combination of an enhanced global precipitation rate and a deficit in the water content of the atmosphere.

HadGEM1 and HadGEM2-AO show a substantial reduction in the evaporation over the tropical-subtropical Atlantic, a distinct error in HadCM3. Previous work (Latif et al. 2000; Thorpe et al. 2001) has shown that the THC is potentially sensitive to the Atlantic salinity budget. The over-evaporative tropical Atlantic in HadCM3 becomes even more strongly evaporative in a greenhouse-warmed world. This leads to a build up of more saline water, which on advection to the north supports deep convection, increases the steric gradient, and tends to stabilise the THC. A broadly similar response is found in Latif et al. (2000), though in their case it is associated with preferential excitation of an El Niño-like response under enhanced greenhouse forcing. It is an open question as to whether the errors in model physics that are responsible for the overly evaporative tropical Atlantic in HadCM3 are also implicated in the strongly stabilising nature of salinity advection in the model, and hence whether the THC in HadCM3 is too stable. On the basis of the salinity advection feedback seen in other models and the reduced evaporative errors in the tropical Atlantic of HadGEM1 and HadGEM2-AO, we would expect the latter two models to exhibit more sensitive THC responses to greenhouse forcing than HadCM3.

Acknowledgments This work was supported by the Joint DECC and Defra Integrated Climate Programme - DECC/Defra (GA01101). We thank John Edwards for his help and suggestions. We also thank Anne Pardaens for comments on the manuscript and Eleanor Burke for providing observational data. We acknowledge the producers of data used in this study for the availability of their datasets. ERA40 data were obtained from the ECMWF data server. NCAR-NCEP reanalysis were obtained from the web site of the climate analysis section at NCAR at <http://www.cgd.ucar.edu/cas/catalog>. NOC climatology was obtained from the National Oceanography Centre's website at http://www.noc.soton.ac.uk/noc_flux. The GSSTF2.0 climatology was obtained from the Distributed Active Archive Centre (DAAC) at <http://daac.gsfc.nasa.gov>. River discharge climatologies were obtained from the Global Runoff Data Centre website at http://www.bafg.de/cln_016/nn_294838/GRDC/EN/Home/homepag. We would like to thank the reviewers for their helpful comments.

References

- Adler RF, Huffman GJ, Chang A, Ferraro R, Xie P, Janowiak J, Rudolf B, Schneider U, Curtis S, Bolvin D, Gruber A, Susskind J, Arkin P (2003) The version 2 global precipitation climatology project (gpcp) monthly precipitation analysis (1979-present). *J Hydrometeorol* 4:1147–1167
- Baumgartner A, Reichel E (1975) *The world water balance*. Elsevier, Amsterdam
- Bosilovich MG, Schubert SD, Walker GK (2005) Global changes of the water cycle intensity. *J Clim* 18:1591–1608
- Bryan K (1969) A numerical method for the study of the circulation of the world ocean. *J Comput Phys* 4:347–376
- Chahine MT (1992) The hydrological cycle and its influence on climate. *Nature* 359:373–380
- Chen TC, Pfaendner J, Weng SP (1994) Aspects of the hydrological cycle of the ocean-atmosphere system. *J Phys Oceanogr* 24:1827–1833
- Chou SH, Nelkin E, Ardizzone J, Atlas R, Shie CL (2003) Surface turbulent heat and momentum fluxes over global oceans based on the Goddard satellite retrievals, version 2 (GSSTF). *J Clim* 16:3256–3273
- Chou SH, Nelkin E, Ardizzone J, Atlas R (2004) A comparison of latent heat fluxes over global oceans from four flux products. *J Clim* 17:3973–3989
- Collins WJ, Bellouin N, Doutriaux-Boucher M, Gedney N, Hinton T, Jones CD, Liddicoat S, Martin G, O'Connor F, Rae J, Senior C, Totterdell I, Woodward S, Reichler T, Kim J (2008) Evaluation of the HadGEM2 model. HCTN 74, Met Office Hadley Centre Technical Note, Met Office, FitzRoy Road, Exeter EX1 3PB, UK
- Cox MD (1984) A primitive equation, three dimensional model of the ocean. Ocean group technical report 1, GFDL, Princeton
- da Silva AM, Young CC, Levitus S (1994) *Atlas of surface marine data, vol. 1: algorithms and procedures*
- Dai A, Trenberth KE (2002) Estimates of freshwater discharge from continents: latitudinal and seasonal variations. *J Hydrometeorol* 3:660–687
- Dodd JP, James IN (1996) Diagnosing the global hydrological cycle from routine atmospheric analyses. *Q J R Meteorol Soc* 122:1475–1499
- Edwards JM (2007) Oceanic latent heat fluxes: consistency with the atmospheric hydrological and energy cycles and general circulation modeling. *J Geophys Res* 112:D06,115. doi:10.1029/2006JD007324
- Fekete BM, Vörösmarty CJ, Grabs W (2002) High-resolution fields of global runoff combining observed river discharge and simulated water balances. *Global Biogeochem Cycles* 16(3):1042. doi:10.1029/1999GB001254
- Global Runoff Data Centre (2009) *Surface freshwater fluxes into the world oceans*. Global Runoff Data Centre. Koblenz, Federal Institute of Hydrology (BfG)
- Gordon C, Cooper C, Senior CA, Banks H, Gregory JM, Johns TC, Mitchell JFB, Wood RA (2000) The simulation of SST, sea ice extents and ocean heat transports in a version of the Hadley Centre coupled model without flux adjustments. *Clim Dyn* 16:147–168
- Grist JP, Josey SA (2003) Inverse analysis adjustment of the SOC air-sea flux climatology using ocean heat transport constraints. *J Clim* 16:3274–3295
- Held IM, Soden BJ (2006) Robust responses of the hydrological cycle to global warming. *J Clim* 19:5686–5699
- Hunke EC, Lipscomb WH (2004) CICE: The Los Alamos sea ice model, documentation and software. Version 3.1. technical report. LA-CC-98-16, Los Alamos National Laboratory, Los Alamos, NM
- Johns TC, Durman CF, Banks HT, Roberts MJ, McLaren AJ, Ridley JK, Senior CA, Williams KD, Jones A, Rickard GJ, Cusack S, Ingram WJ, Crucifix M, Sexton DMH, Joshi MM, Dong BW, Spencer H, Hill RSR, Gregory JM, Keen AB, Pardaens AK, Lowe JA, Bodas-Salcedo A, Stark S, Searl Y (2006) The new Hadley Centre climate model HadGEM1: evaluation of coupled simulations. *J Clim* 19(7):1327–1353
- Josey SA, Kent EC, Taylor PK (1999) New insights into the ocean heat budget closure problem from analysis of the SOC air-sea flux climatology. *J Clim* 12:2856–2880
- Kalnay E, Kanamitsu M, Kistler R, Collins W, Deaven D, Gandin L, Iredell M, Saha S, White G, Woollen J, Zhu Y, Chelliah M, Ebisuzaki W, Higgins W, Janowiak J, Mo KC, Ropelewski C, Wang J, Leetmaa A, Reynolds R, Jenne R, Joseph D (1996) The NCEP/NCAR 40-year reanalysis project. *Bull Am Meteorol Soc* 77(3):437–471
- Latif M, Roeckner E, Mikolajewicz U, Voss R (2000) Tropical stabilisation of the thermohaline circulation in a greenhouse warming simulation. *J Clim* 13:1809–1813
- Martin GM, Ringer MA, Pope VD, Jones A, Dearden C, Hinton TJ (2006) The physical properties of the atmosphere in the new Hadley centre global environmental model, (HadGEM1). Part I: model description and global climatology. *J Clim* 19:1274–1301. doi:10.1175/JCLI3636.1
- Mitchell KE, Lohmann D, Houser PR, Wood EF, Schaake JC, Robock A, Cosgrove BA, Sheffield J, Duan Q, Luo L, Higgins RW, Pinker RT, Tarpley JD, Lettenmaier DP, Marshall CH, Entin JK, Pan M, Shi W, Koren V, Meng J, Ramsay BH, Bailey AA (2004) The multi-institution North American land data assimilation system (NLDAS): utilizing multiple GCIP products and partners in a continental distributed hydrological modeling system. *J Geophys Res* 109:D07S90. doi:10.1029/2003JD003823
- Oki T (1999) The global water cycle. In: Browning KA, Gurney RJ (eds) *Global energy and water cycles*. Cambridge University Press, pp 10–29
- Oki T, Sud YC (1998) Design of total runoff integrating pathways (TRIP) — a global river channel network. *Earth Interact* 2:1–37
- Pardaens AK, Banks HT, Gregory JM, Rowntree PR (2003) Freshwater transports in HadCM3. *Clim Dyn* 21:177–195
- Park YG (1999) The stability of thermohaline circulation in a two-box model. *J Phys Oceanogr* 29:3101–3110
- Peixoto JP, Oort AH (1992) *Physics of climate*. American Institute of Physics, New York, p 520
- Pope VD, Gallani ML, Rowntree PR, Stratton RA (2000) The impact of new physical parametrizations in the Hadley Centre climate model—HadAM3. *Clim Dyn* 16:123–146

- Randel DL, Vonder Haar TH, Ringerud MA, Stephens GL, Greenwald TJ, Combs CL (1996) A new global water vapor dataset. *Bull Am Meteorol Soc* 77:1233–1246
- Ringer MA, Martin G, Greeves C, Hinton T, James P, Pope V, Scaife A, Stratton R, Inness P, Slingo J, Yang GY (2006) The physical properties of the atmosphere in the new Hadley centre global environmental model (HadGEM1). Part II: aspects of variability and regional climate. *J Clim* 19(7):1302–1326
- Semtner AJ (1976) A model for the thermodynamic growth of sea ice in numerical investigations of climate. *J Phys Oceanogr* 6:379–389
- Thorpe RB, Gregory JM, Johns TC, Wood RA, Mitchell JFB (2001) Mechanisms determining the Atlantic thermohaline circulation response to greenhouse gas forcing in a non-flux-adjusted coupled climate model. *J Clim* 14:3102–3116
- Trenberth KE (1997) Using atmospheric budgets as a constraint on surface fluxes. *J Clim* 10:2796–2809
- Trenberth KE, Smith L, Qian T, Dai A, Fasullo J (2007) Estimates of the global water budget and its annual cycle using observational and model data. *J Hydrometeorol* 8:758–769
- Uppala SM, Kållberg PW, Simmons AJ, Andrae U, da Costa Bechtold V, Fiorino M, Gibson JK, Haseler J, Hernandez A, Kelly GA, Li X, Onogi K, Saarinen S, Sokka N, Allan RP, Andersson E, Arpe K, Balmaseda MA, Beljaars ACM, van de Berg L, Bidlot J, Bormann N, Caires S, Chevallier F, Dethof A, Dragosavac M, Fisher M, Fuentes M, Hagemann S, Hólm E, Hoskins BJ, Isaksen I, Janssen PAEM, Jenne R, McNally AP, Mahfouf JF, Morcrette JJ, Rayner NA, Saunders RW, Simon P, Sterl A, Trenberth KE, Untch A, Vasiljevic D, Viterbo P, Woollen J (2005) The ERA-40 re-analysis. *Q J R Meteorol Soc* 131:2961–3012. doi:[10.1256/qj.04.176](https://doi.org/10.1256/qj.04.176)
- Xie P, Arkin PA (1997) Global precipitation: a 17-year monthly analysis based on gauge observations, satellite estimates and numerical model outputs. *Bull Am Meteorol Soc* 78(11):2539–2558